Chapter 14
Tellurite glass fibers for mid-infrared nonlinear applications

Xian Feng, Peter Horak, Francesco Poletti

Optoelectronics Research Centre

University of Southampton

Highfield, Southampton

United Kingdom, SO17 1BJ

Abstract In this chapter, we will review the progress of using tellurite glass nonlinear fibers for mid-infrared nonlinear applications in this chapter. First, we introduce various fabrication approaches for making conventional solid core/clad tellurite glass preforms and structured tellurite glass preforms. Second, two technical difficulties have been found during the early stage of using small-core tellurite glass fiber for generating nonlinear supercontinuum into mid-infrared region. Approaches such as glass dehydration and large-mode-area fiber have been developed for solving these problems.

1 Introduction

The mid-infrared (mid-IR) 2-5 μm and 8-13 μm regions are the two atmospheric transmission windows, where the Earth's atmosphere is relatively transparent. These two windows are important for using remote laser sensing for the atmospheric, security and industrial applications such as detecting remote explosives, countermeasures against heat-seeking missiles and covert communication systems [1]. A broadband or tunable laser source with medium or high average power level (100 mW-10 W) ranging between 2-5 μm is thus highly demanded. Unfortunately, the commonly used active laser sources, e.g., transition metal ions doped chalcogenide crystal lasers, quantum cascade lasers, and rare earth doped fluoride fiber lasers, are not able to completely cover the whole range. For example, the state-of-the-art Cr(II):ZnSe tunable laser can only cover the range of 1.97-3.35 μm [2] and the state-of-the-art Fe(II):ZnSe tunable laser can only cover the range of 3.95-5.05 μm [3]; for quantum cascade laser, 3 μm is the short wavelength limit due to the

material limitations such as conduction band offset [4,5]; mid-IR rare-earth-doped fluoride fiber lasers can provide relatively narrow-line emission discrete spectra in the range of 2-4 μm, because the phonon energy (500-600 cm^{-1}) of fluoride glass hosts is still not low enough for lasing at longer wavelengths and the emission wavelengths because 4f-4f electron transitions of a certain type of rare earth ions are not very sensitive to the glass host [6,7].

Instead, $\chi^{(2)}$ nonlinear crystal optical parametric oscillator (OPO) is one of the most commonly used approaches for generating widely tunable output covering the whole 2-5 μm range [8]. But for achieving medium or high average power level (100 mW-10 W) and wide wavelength tunability, the volume of an OPO is normally large and complicated optical configurations are required.

On the other hand, the recent progress in tailored low-dispersion highly-nonlinear photonic crystal fibers (PCFs, also called as microstructured optical fibers) [9] has shown that fiber-based $\chi^{(3)}$ nonlinear laser sources, such as the supercontinuum [10], fiber OPO [11], or frequency comb [12] can also fulfil this task. What is more, fiber lasers show significant advantages over other solid state lasers as an effective approach to provide economic, compact and flexible optical components. Also excellent beam quality can be obtained from a single mode fiber.

2-5 μm mid-IR nonlinear lasers requires a nonlinear glass with high transparence in 2-5 μm to be the fiber host material. The position of the IR absorption edge, i.e., the infrared longwave transmission limit, of an optical glass is intrinsically limited by the multiphonon absorption edge of the glass. This can be simply explained by Hooke's law using the two-mass spring model [13]. In general, non-silica glasses, such as tellurite (TeO_2 based), fluoride (typically ZrF_4 or AlF_3 based), and chalcogenide (chalcogen S, Se, Te based) glasses [14-16], possess excellent optical transparence in the wavelength range of 0.5-5 μm, 0.4-6 μm and 1-16 μm respectively and thus are attractive candidates as fiber materials for mid-infrared applications over the conventional silica. The latter shows inferior transparence beyond 2 μm, due to (i) the strong fundamental vibration hydroxyl absorption at 2.7 μm and (ii) high loss (>50 dB/m) starting from 3 μm due to the tail of the multi-phonon absorption of Si-O network.

For realizing such a fiber-based compact 2-5 μm mid-IR nonlinear laser, the conventional high-power or high-energy continuous wave (CW) or pulsed erbium, thulium or holmium doped fiber lasers with the lasing wavelength at 1.5 μm or 2 μm, are ideal as the pump source. This requires the nonlinear fiber having a zero dispersion wavelength at 1.5 or 2 μm in order to maximize the efficiency of nonlinear frequency conversion.

Tellurite glasses have been considered as one of the promising candidates of the fiber materials for mid-infrared applications since 1980 [14]. In the very first work using tellurite fibers for mid-IR applications, it was found that in the range of 2-5 μm, the selected tellurite glass unclad fiber on the composition of $70TeO_2$-20ZnO-10BaO (mol.%) showed reasonably low losses up to 40 dB/m, which was not useful for long-haul applications at that time but still attractive enough for short-haul applications [14].

Figure 1 illustrates the statistical relation between the linear refractive index n and nonlinear refractive index n_2 of various optical glasses.

Table 1 compares the key physical and chemical properties of various optical glasses, including silica, tellurite, fluoride and chalcogenide glasses, as the candidates for mid-IR nonlinear applications.

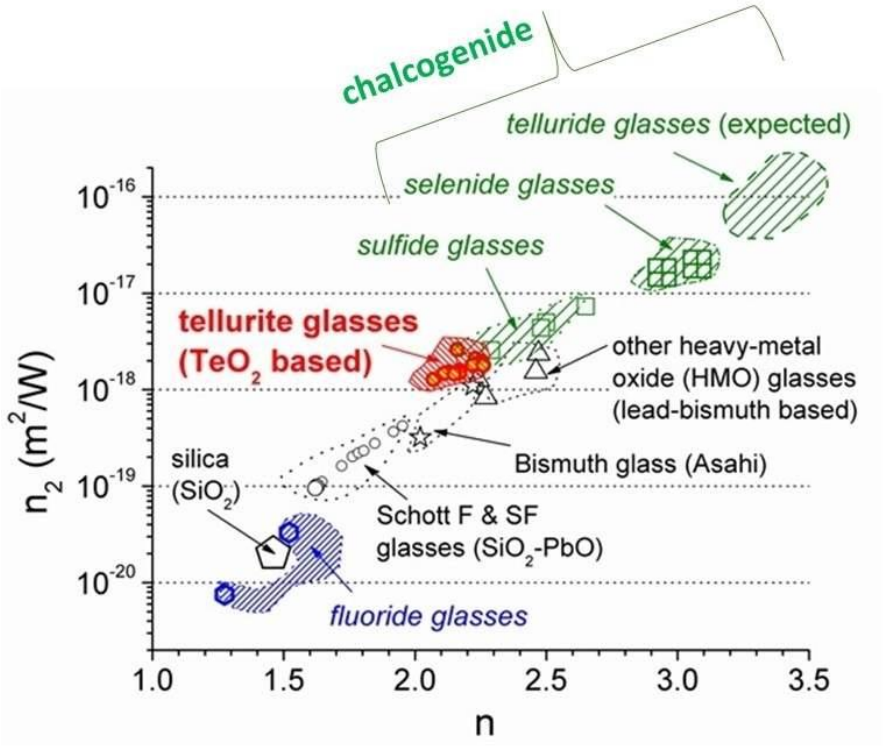

Fig. 1. Relation between the linear refractive index n and nonlinear refractive index n2 in various optical glasses

Technically, tellurite glasses can be regarded as a high-index, highly nonlinear version of fluoride glasses. Both tellurite and fluoride glasses possess (i) steep viscosity curve around the fiber drawing temperature [17], (ii) the zero dispersion wavelength of the bulk material of ~2μm [18], and (iii) longwave transmission limit (6-7 μm for the bulk). As shown in Fig.1, tellurite glasses have high refractive index n (2.0-2.2) and nonlinear refractive index n_2 (20-50 x 10^{-20} m^2/W), while fluoride glasses typically have n of ~1.5 and n_2 of ~2 x 10^{-20} m^2/W, as low as silica glass.

Another rival for 2-5μm mid-IR nonlinear applications is chalcogenide glasses, which is a glass family based on chalcogen elements (S, Se and Te). Chalcogenide glasses possess high n_2 of 100-1000 x 10^{-20} m^2/W, which is 2-3 order higher than

that of tellurite glasses and show excellent IR transmission up to 16 μm, superior to tellurite and fluoride glasses. These outstanding performances make chalcogenide glasses a very promising host material as $\chi^{(3)}$-based highly nonlinear fiber media. However, the material zero dispersion wavelength of chalcogenide glasses is beyond 5μm.

In order to make the zero dispersion wavelength of a chalcogenide glass fiber close to 1.5 or 2 μm, very large waveguide dispersions need to be introduced, requiring the final fiber core diameter to be submicron. This is disadvantageous for power scaling because such a small-core fiber suffers from low damage threshold power. Hence, tellurite glasses are an ideal host material as a fiber nonlinear medium for 2-5μm wavelength range.

Table 1. Comparison of various optical glasses as host materials for mid-infrared nonlinear fibers [14–24]

	Silica	Tellurite	Fluoride	Chalcogenide
Refractive index n at 1.55 μm	1.46	2–2.2	~1.5	2.3–3
Nonlinear refractive index n_2 ($\times 10^{-20}$ m^2/W)	2.5	20–50	2–3	100–1000
Raman gain coefficient g_R at 1.064μm ($x10^{-11}$ cm/W)	0.93	32	1.1±0.3	280-720
Raman shift (cm^{-1})	440	650-750	550	250-350
λ_0, zero dispersion wavelength of material (μm)	~1.3	~2	~1.7	>5
IR longwave transmission limit	up to 3 μm	6–7 μm	7–8 μm	12–16 μm
Reported lowest loss dB/m (wavelength)	$0.15x10^{-3}$ (1.55 μm)	0.0204 (1.56 μm)	$0.45x10^{-3}$ (2.35 μm)	0.023 (2.3 μm)
Thermal stability for fiber drawing	excellent	good	poor	good
Viscosity around fiber drawing temperature	flat	steep	steep	flat
Durability in environment	excellent	good	poor, hygroscopic	good
Toxicity	safe	safe	relatively high	relatively high

In addition, as shown in Table 1, tellurite glass is chemically durable in the environment for usage and less toxic due to its oxide nature, compared with other two families of non-oxide glasses.

In principle, broadband mid-IR supercontinuum or other nonlinear processes such as four-wave-mixing (FWM) based nonlinear parametric generation can be realized using a single-mode large-mode-area (LMA) tellurite fiber pumped with a high-power CW or pulsed 2 μm thulium (Tm^{3+}) or holimium (Ho^{3+}) doped fiber laser [19]. But, due to the strong water absorption (~1400 dB/m or ~4 cm^{-1}) peaking at 3.3 μm, this makes even an 8mm-long 'wet' tellurite glass fiber suffer a 15-20 dB loss in light intensity around 3-4 μm and leads into very poor nonlinear conversion efficiency in 3-5 μm region [20]. Since the tail of multiphonon absorption of tellurite glasses starts from ~5 μm, dehydration is the key approach to extend the high transmission window (i.e., absorption coefficient <0.1 cm^{-1}) of a tellurite glass fiber into the range of 3-5 μm.

In this chapter, we first introduce various fabrication approaches for making preforms for solid core/cladding fiber and microstructured photonic crystal fibers, the selection of the glass compositions for the host materials of the fibers, and the dehydration of the tellurite glass for having low loss in the mid-IR region. From the early works on using small-core, dispersion-tailored tellurite fibers for generating mid-IR supercontinuum, the power scaling and the huge water induced impurity attenuation at 3-4 μm band are found to be the two major technical difficulties. To overcome these two problems, further works on using (i) dehydrated small-core and (ii) large-mode-area (LMA) tellurite photonic crystal fibers have then been carried out.

2 Fabrication

Making fiber preform is the most important process to realize the targeted fiber with decent attenuation.

Casting method has been previously developed for making all-solid fiber with core/cladding structure [25-29]. On the other hand, for making non-silica glass microstructured preform for photonic crystal fiber, extrusion, ultrasonic drilling and capillary stacking are the typical approached [30]. Since the ultrasonic drilling and capillary stacking tend to introduce surface defects and/or water impurity onto the holes of the fabricated preforms during the processing, here we mainly focus on the casting method and the extrusion method.

2.1 Preform fabrication

Built-in casting method is a traditional method for making solid core/cladding preform, which was developed initially for making low-loss fluoride glass fiber preform in the early 1980s [25]. First, a cladding glass tube is obtained by casting the cladding glass in a preheated metal mould. The mould is then overturned immediately and the unsolidified melt in the center of the mould flows out. Casting the core glass into the cladding tube, the core/cladding preform is then obtained. The great advantage of this method is the good optical quality of the core/clad interface. Fluoride fibers with low losses of 1 dB/km have been drawn from preforms prepared by this method [26]. However, long length fibers with a uniform core diameter along the fiber are difficult to be achieved, because the preform typically shows tapered core dimensions along the length.

A modified build-in casting technique has then been proposed [27]. A hole is made in the bottom plate of the mould. The cladding glass melt is first cast into a pre-heated metal mould. The core glass melt is then cast onto the cladding glass tube, before the central part of the cladding glass gets solidified. The mould is then moved to make the central part of molten glass flowing down through the hole in the bottom plate. The core glass melt takes place at the central part of the cladding glass, to form the core/cladding structure (see Fig.2). Generally, the core/clad diameter ratio is in a narrow range between 0.5 and 0.6 [27].

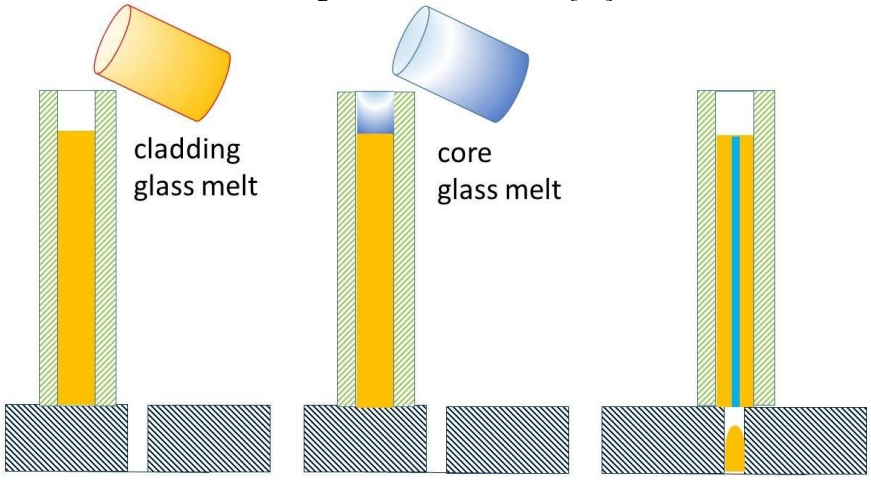

Fig. 2. Schematic of modified built-in casting method

Rotational casting method is another approach to make core/cladding structured preform [28]. The cladding tube is prepared by pouring the cladding melt into a cylindrical mould. The mould is then immediately rotated at a speed ranging above 1000 rpm for a few seconds. Using this technique, the inner diameter of the cladding tube can be easily controlled by adjusting the volume of glass melt for a

given mould. Fiber drawn from preform prepared by this method gives transmission losses of about 1 dB/km in fluoride glass fibers [29].

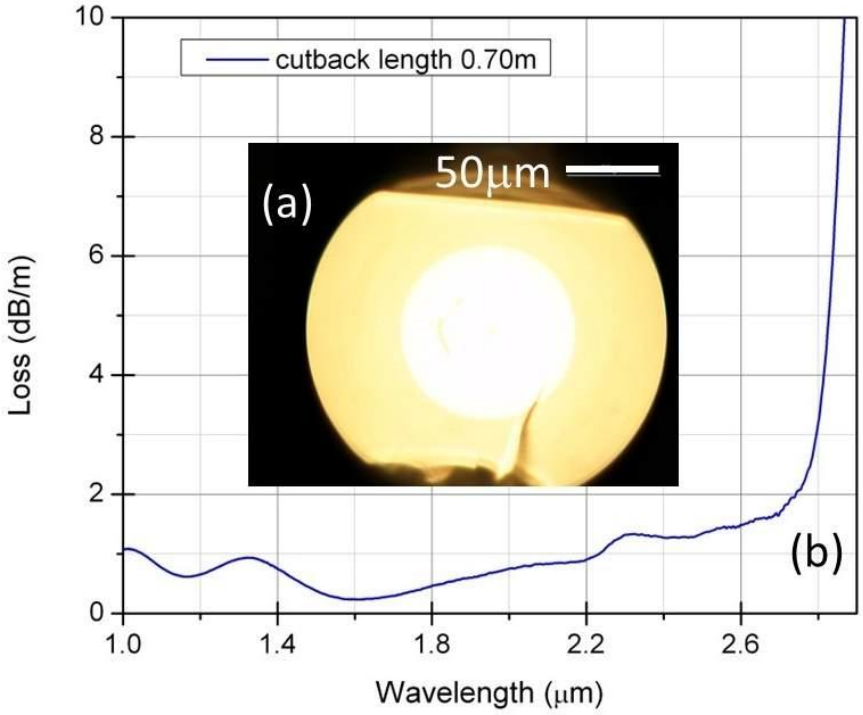

Fig. 3. (a) Optical photograph of a fabricated tellurite glass multimode fiber from a core/cladding preform made by modified built-in casting method; (b) Measured loss spectrum using cutback method with cutback length of 0.70 m.

Fig.3 (a) shows the photograph of one of our fabricated tellurite glass multimode fiber from a core/cladding preform made by modified built-in casting method. The fiber has a core diameter of 90 μm and an OD of 190 μm. The numerical aperture (NA) of the fiber is ~0.25. The fiber is based on the composition of $75TeO_2$-$20ZnO$-$5Na_2O$ (mol.%). As one can see in Fig.3(b), the loss of the multimode fiber drawn from the preform is measured to be between 0.4-1.5 dB/m in the range of 1.0-2.6 μm. The loss of the fiber increases dramatically beyond 2.7 μm due to the absorption of water impurity inside the glass.

2.2 Fabrication of structured preforms for tellurite photonic crystal fibers

The extrusion technique is a traditional method for making glass workpiece with simple or complex geometry [31]. As shown schematically in Fig.4, the solid glass billet is first loaded inside a metal sleeve. The glass is then heated above the glass softening temperature and high pressure is applied onto the glass billet through a metal ram, forcing the viscous glass flow passing through the channels inside extrusion die. The glass flow forms a preform with the structure opposite to the structure on the die. This technique is especially suitable for making glass workpieces based on those glasses with a short operating range (known as short glasses) or glasses with high tendency for crystallization [31].

Fig.5 (a)-(c) illustrate optical photographs of some extruded tellurite glass preforms. The tellurite glass is with the composition of $75TeO_2$-$20ZnO$-$5Na_2O$ (mol.%). It is seen that the extrusion method is indeed a powerful tool for making preforms with simple geometry such as rods and tubes, as well as preforms with complex structure such as multiple holey structures or air-suspended core. In particular, from Fig.5(c), one can see that the supporting glass spokes have the thickness of 30 μm and the length of 1.7 mm, which are obviously very difficult features to be made by any other known approaches.

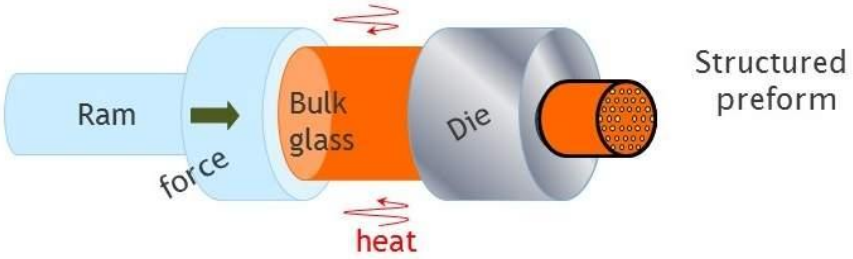

Fig. 4. Schematic plot of making structured preform using glass extrusion method

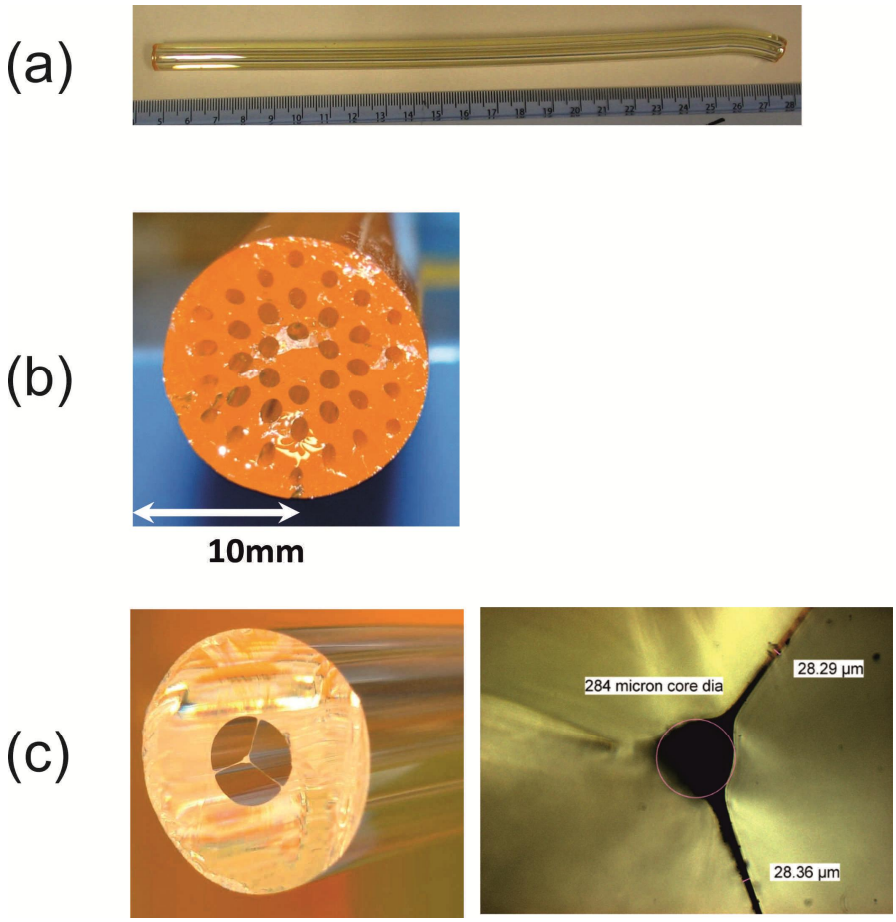

Fig. 5. Optical photographs of some extruded tellurite glass preforms. The tellurite glass has composition $75TeO_2$-$20ZnO$-$5Na_2O$ (mol.%). (a) Side view of an extruded tube with OD of 10.0 mm and inner diameter (ID) of 2.0 mm. (b) Cross-sectional view of an extruded structured preform with multiple holes around a solid core. (c) Cross-sectional view of an extruded preform with a suspended core. The preform has a diameter of 9.7 mm. A suspended core is supported by three thin and long glass spokes. The spokes have the length of 1.7 mm. The core diameter and the thickness of the supporting spokes on the preform is 284 µm and 28 µm.

2.3 Fiber fabrication

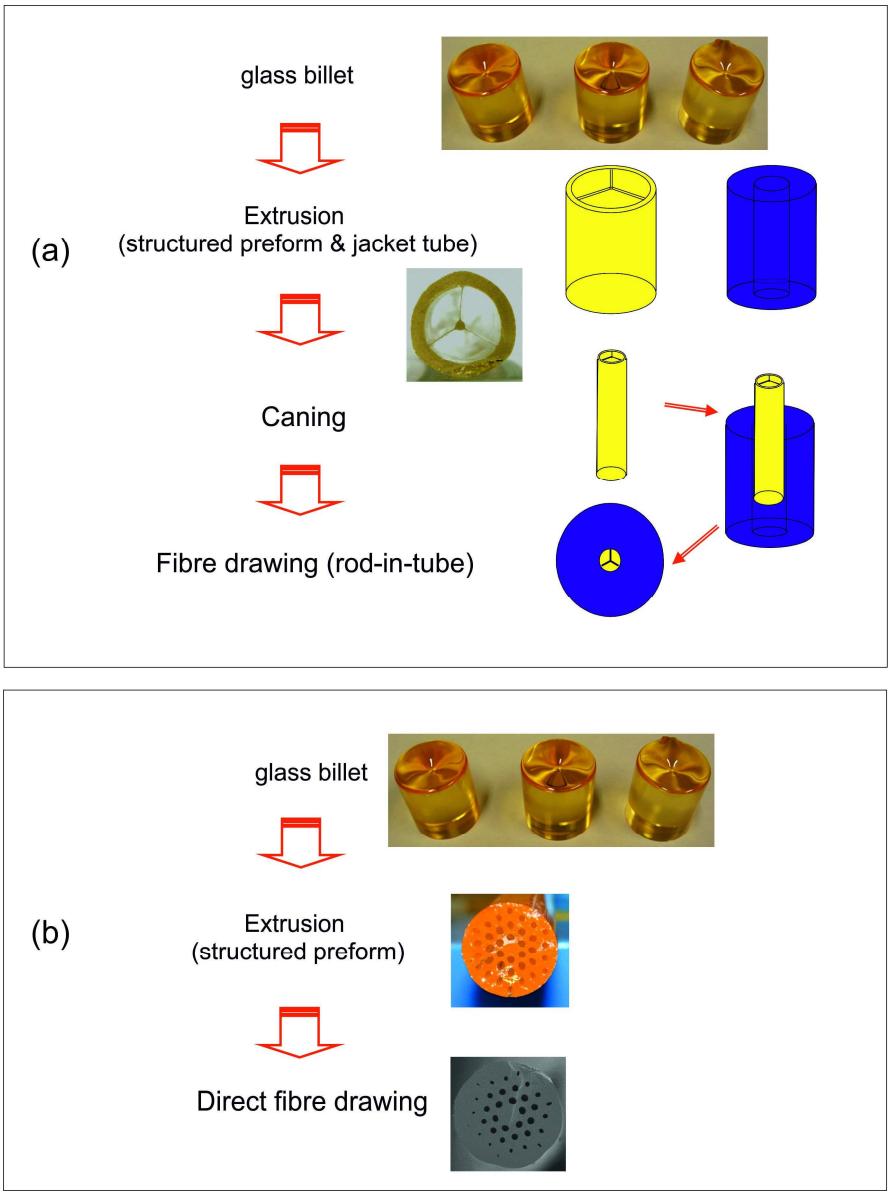

Fig. 6. Flow chart of fabricating (a) small-core and (b) large-core tellurite PCF, starting from extrusion

Fiber fabrication is the procedure to reduce the size of preforms from tens of millimeters down to hundreds of microns. The reduction ratio is the key parameter that a fabricator must consider in the fiber drawing. If the reduction ratio from the outer diameter (OD) of the preform to the OD the fiber is much larger than the ratio between the core diameter on the preform and the core diameter on the fiber, a second step of the fiber drawing will be necessary. For example, for a preform with an OD of 12.5 mm and a core diameter of 1.0 mm, one step of fiber drawing is enough to obtain a fiber with a core diameter of 10 μm. But if the targeted core diameter is 1.0 μm, another step of fiber drawing is then required.

Fig.6 (a) shows the flow chart of making a small-core tellurite PCF, using the extrusion method. First, the cylindrical glass billets with a diameter of 29 mm and a height of ~35 mm are made by conventional melting-casting method. The purity of the raw chemicals was at least 4N (99.99%). The preform with a suspended core is then extruded. The structured preform is then elongated to a small cane. The cane is then inserted inside an extruded jacket tube with an inner diameter slightly larger than the outer diameter of the cane. The set of cane and tube is finally drawn into the fiber. Given the reduction ratio at the last step of fiber drawing is in the range of 100-200, the final core diameter will be between 1 and 2 μm. The yield of a fiber draw is typically more than a hundred of meters in length.

Fig.6 (b) shows the flow chart of making large-core tellurite PCF, using the extrusion method. After extrusion, the structured preform can be directly drawn into fiber, since the reduction ratio from the preform to the fiber is less than 100.

3. Selection of glass compositions as fiber host

After the pioneering systematical works of J. E. Stanworth [32] on tellurite glasses, it has been noticed that TeO_2-ZnO and TeO_2-WO_3 are the two glasses candidates with the large glass forming area amongst all tellurite glass compositions [33]. Large glass forming area indicates that (i) it is easy to find a few glass compositions with good thermal stability in the forming area and (ii) it is relatively easy to find one pair of glass compositions with acceptable thermal mismatch and good thermal stability as the core and cladding. This is the reason why, in the later works on tellurite glass fibers, TeO_2-ZnO-Na_2O [23], TeO_2-ZnO-BaO [14] and TeO_2-WO_3-La_2O_3 [34, 35] are the most preferable compositions.

The thermal stability of a fiber host glass is important for the fabrication, in particular when multiple steps of thermal processing (i.e., extrusion, caning and fiber drawing) are required. Fig.7 illustrates the measured differential thermal analysis (DTA) curve and the measured glass viscosity curve of selected glass composition of 75TeO_2-20ZnO-5Na_2O glass (mol.%), in which T_g and T_x are the temperatures of glass transition and the onset of crystallization, respectively. Since the usable viscosity ranges for preform-extruding and fiber-drawing are 10^9-$10^{7.5}$ poise and $10^{6.5}$-10^4 poise, respectively, crystallization will not occur even when

the glass is processed at the upper limit of working temperature, corresponding to the lower viscosity limit for fiber-drawing. This indicates the excellent thermal stability of this glass for fiber fabrication.

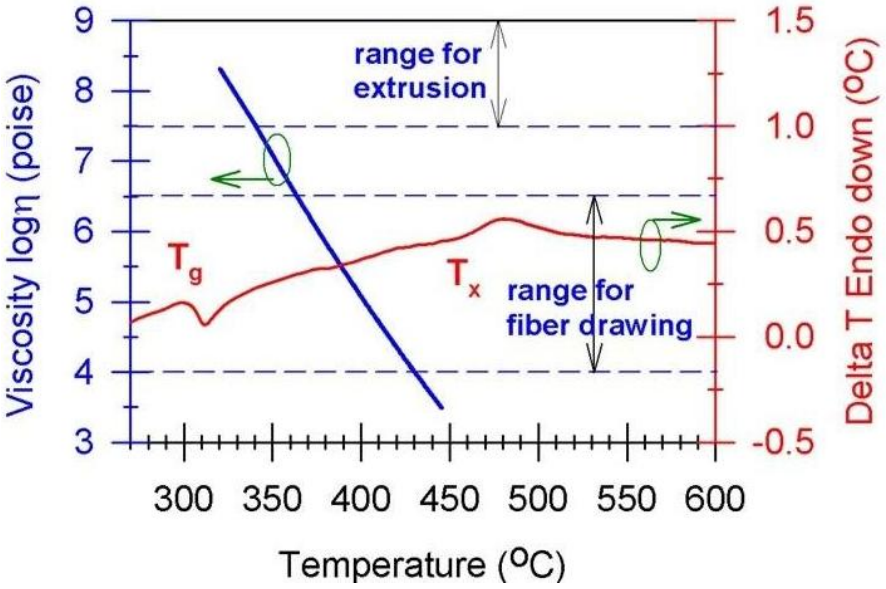

Fig. 7. DTA curve and viscosity curve of selected $75TeO_2$-$20ZnO$-$5Na_2O$ glass (mol.%)

In this chapter, we mainly focus on two tellurite glass compositions, $75TeO_2$-$20ZnO$-$5Na_2O$ glass (mol.%) and $70TeO_2$-$20ZnO$-$10BaO$ (mol.%) as the host materials of fibers. Table 2 summarizes the major thermal properties of these two glass compositions. It is seen that both compositions have large difference between T_g and T_x, indicating excellent thermal stability for glass extrusion and fiber drawing.

Table 2. Thermal properties of $75TeO_2$-$20ZnO$-$5Na_2O$ glass (mol.%) and $70TeO_2$-$20ZnO$-$10BaO$ (mol.%)

Glass composition (mol.%)	T_g (°C)	T_x (°C)	$\Delta T(=T_x - T_g)$ (°C)
$75TeO_2$-$20ZnO$-$5Na_2O$	305	465	160
$70TeO_2$-$20ZnO$-$10BaO$	320	/	∞

The typical impurities in an optical glass are transition metal ions, rare-earth ions, and hydroxyl groups (the OH groups). Because the purity of the raw chemicals for melting tellurite glasses here is 4-5N (99.99%-99.999%), the total impurities in the final glass ought to be at 10-100ppm.

4. Impurities in tellurite glasses and glass dehydration

Transition metal ions, rare earth ions and hydroxyl groups are the three major categories of impurities having big impact on increasing attenuation of optical glasses in the wide range from visible wavelengths to mid-infrared region.

Based on the data given in Ref. [36], Fig. 8 shows the measured transmission spectra of bulk tellurite glasses (base: $75TeO_2$-$20ZnO$-$5Na_2O$, mol.%) doped with the impurities including the representative transition metal ion Ni^{2+}, the representative rare earth ion Nd^{3+}, and the hydroxyl group OH^-. It is seen that the fundamental vibration of the hydroxyl group OH^- is the most harmful impurity for blocking the transmission of a tellurite glass in 2–5 μm region, in terms of the wide absorption range (3–4 μm) and the high peak absorption coefficient (10 dB/m/ppm).

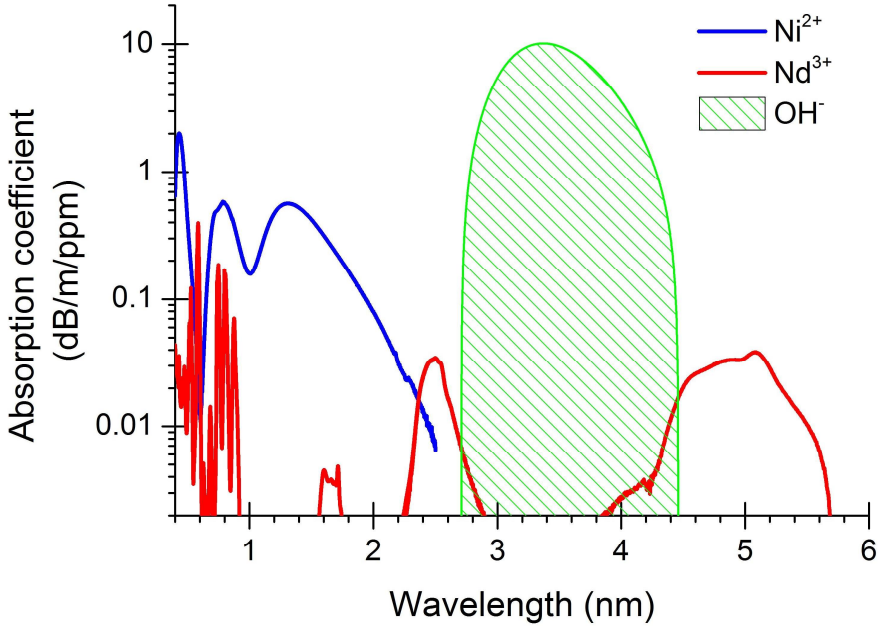

Fig. 8. Comparison of absorption coefficients of some selected impurities in a conventional tellurite glass (composition: $75TeO_2$-$20ZnO$-$5Na_2O$, mol.%) (summarized from results in Reference [36].)

Water, commonly existing in many optical materials as the hydroxyl group OH^-. Although water is the most important substance on the earth for all the living creatures, actually it is a trouble maker in optical area. It causes high attenuation in optical materials from visible to mid-infrared regions. As one of the most common impurities in optical materials, hydroxyl groups OH^- are very hard to be eliminated.

The absorption spectrum of the OH fundamental vibration is located around 3 μm and varies with the glass composition. For pure silica glass, the fundamental vibration of OH band is located at 2.70 (± 0.02) μm and with an extinction coefficient of 10 dB/m/ppm (in weight) [37], while in a ZrF_4-based fluoride glass, it is located at 2.87 μm with an extinction coefficient of 5 dB/m/ppm (in weight) [38]. For a tellurite glass, the fundamental vibration of OH band has an extinction coefficient of ~1 dB/m/ppm (in mole) or ~10 dB/m/ppm (in weight) [39], and ranges from 3 to 4 μm, much wider than the above two glasses. This is because the wavelength of the fundamental OH vibration reflects the strength of OH bonding with the surrounding molecules. The large variety of deformed [TeO_4] and [TeO_3] units in tellurite glass network causes very different sites of OH groups and consequently the bond strength of OH groups shows much larger variation [39]. This is very different from the situation of pure silica glass, in which the [SiO_4] tetrahedra units are very much identical in the short range leading to the fundamental OH absorption as narrow as ~150 nm (~200 cm^{-1}) [37].

Because the nonlinearity n_2 of tellurite glasses is one order of magnitude higher than those of silica and fluoride glasses, less than a meter length of tellurite nonlinear fiber is acceptable for many nonlinear optical applications, indicating that an acceptable OH peak absorption loss is no more than the level of 10 dB/m. In other words, the OH impurity in a usable tellurite glass fiber should be no more than the level of 1 ppm in weight. It must be pointed out that, without any dehydration process, the tellurite glass, which was prepared in the open atmosphere, has a high water absorption coefficient of ~1400 dB/m peaking at 3.4 μm [39]. Therefore, even an 8 mm-long non-dehydrated tellurite glass fiber, will suffer a 15–20 dB loss in the range of 3–4 μm [40]. Since the tail of multiphonon absorption of tellurite glasses starts from ~5 μm, a proper dehydration process is the key to extend the high transmission window (*i.e.*, absorption coefficient < 0.1 cm^{-1}) of a tellurite glass fiber to 5 μm.

Reactive atmosphere processing (RAP) has been proved to be an effective approach for dehydrating fluoride and silica glasses [41, 42]. In the case of dehydrating fluoride glasses, during the melting of fluoride glass, dry reactive halogen gas (such as NF_3, HF, SF_6, and CCl_4) is purged into the melt to react with the OH groups inside the glass [41]. The hydroxyl groups bonded with the glass network via hydrogen bonding are converted into the volatile compounds HF or HCl, which can be removed from the melt naturally at high temperature. Chlorine drying is also a common method in the fabrication of silica glass preforms to reduce the OH peaks at 1.38μm (the first overtone) [41]. For dehydrating tellurite glasses, in order to avoid using highly toxic and reactive halogen gases, halogen-containing solid compounds are preferable. Previously, fluorotellurite glass, obtained by introducing fluorine into the oxide tellurite glass matrix, has been proposed to remove the OH groups with the assistance of fluorine, and also to extend the mid-IR transmission [43]. However, the oxyfluoride glass has strong tendency to be crystallized easily during the heating process and hence is not a thermally stable host material for fiber drawing. Also the introduction of fluorides causes the

glass hygroscopic. In addition, introducing fluorides into tellurite glasses leads into significant decrease of both the refractive index and the nonlinear refractive index [43].

Solid-state chloride compounds, such as NaCl and $BaCl_2$, were then added for dehydrating tellurite glasses [44]. Pyrohydrolysis reaction, $OH^-+Cl^-=HCl+O^{2-}$ $OH^- + Cl^- = HCl \uparrow + O^{2-}$, occurs during the glass melting for reducing the OH content in the glass. The compositions of the studied halo-tellurite glasses include: $75TeO_2$-20ZnO-$5Na_2O$ (TZN), $75TeO_2$-20ZnO-$4Na_2O$-2NaCl (TZNX1), $70TeO_2$-20ZnO-10BaO (TZB), $70TeO_2$-20ZnO-9BaO-$1BaCl_2$ (TZBX1) and $70TeO_2$-20ZnO-$10BaCl_2$ (TZBX10) (mol.%). Commercial chemicals with purity better than 99.999% were used as raw materials for the glass melting. For each composition, a batch of 70 g was mixed well and then melted in a gold crucible inside a furnace in the glovebox at 700-900 ^oC for 2 hours. Increasing the melting time in dry atmosphere was found helpful to reduce the OH content in the glass. But it also caused the deviation of the final glass composition from the targeted one when the melting time is longer than 3 hours, since significant evaporation could be observed from tellurite glass melt. The melt was then cast in a preheated metal mold, and a bubble-free glass rod with an outer diameter (OD) of 16 mm and length between 45-65 mm was obtained. Each rod was drawn into an unclad fiber with an OD of 180 μm, with the yield >50 m. A bulk sample was then obtained from the preform remainder with two parallel ends polished.

The transmission spectrum of each bulk was measured by a Varian 670-IR FT-IR spectrometer. The absorption coefficient (in the unit of cm^{-1}) of the residual OH impurity in the bulk glass was calculated according to the Beer–Lambert law and converted to the bulk attenuation in dB/m. The losses of the unclad fibers were measured by the cutback method, using a tunable 1064 nm nanosecond laser pumped periodically lithium niobate (MgO:PPLN) (Covesion Ltd) as the laser source [44, 45]. Essentially, the unclad fiber drawn from a dehydrated TZNX1 glass (i.e., using 2 mol.% of NaCl to replace 1 mol.% of Na_2O in TZN glass) rod showed a largely reduced loss of 45 dB/m at 3.3 μm [44, 45], compared with the loss of ~1400 dB/m at 3.3 μm in a TZN glass melted in the open atmosphere [39] and the loss of 100 dB/m of a TZN glass melted in a dry atmosphere filled glovebox [46].

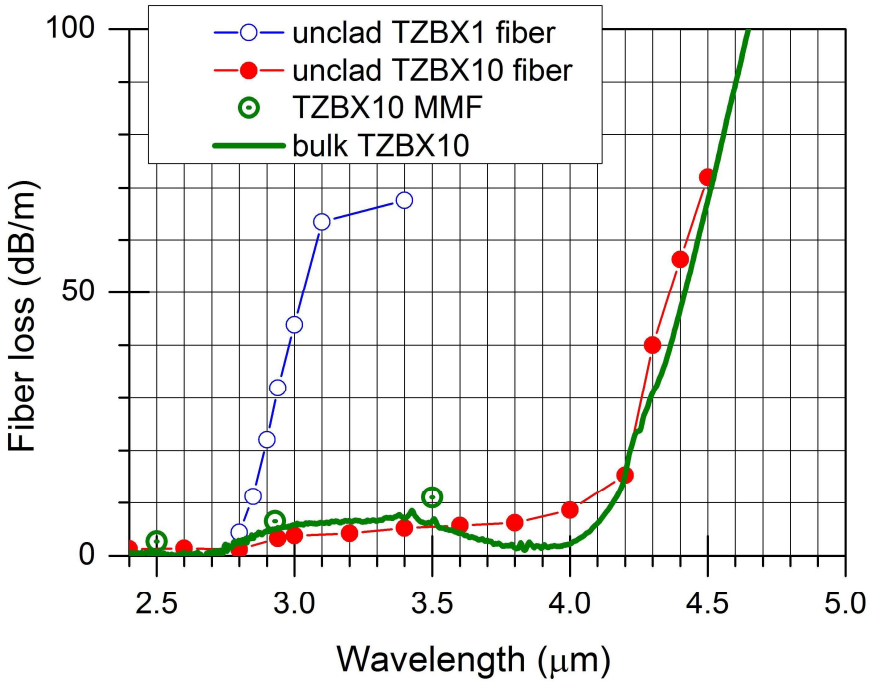

Fig. 9. Losses of dehydrated TZBX glass and fibers in mid-IR region

As shown in Table 2 in this chapter, the TZB glass shows better thermal stability than the TZN glass, indicating it also a good fiber host material. Fig. 9 shows our latest improvement on measured mid-IR losses from dehydrated TZBX glass fibers. It is seen that the losses of the dehydrated TZBX10 unclad fiber at 3.3-3.4 μm is reduced down to 5 dB/m, about one order of magnitude lower than those of the dehydrated TZBX1 unclad fiber at the same wavelengths. The OH impurity level here is estimated to be 0.5 wt. ppm. In a TZBX10 based multimode fiber with a core diameter 60 μm and an NA of 0.14, the losses in the same wavelength region are still below 10dB/m. The interface imperfections between the core and the cladding in the multimode fiber are responsible for the loss increase above the unclad fiber. Further improvement on the preform fabrication should be able to solve this problem. It is seen that the loss curves of the unclad TZBX10 fiber and TZBX10 bulk show the good agreement beyond 4.2 μm, where the multiphonon absorption edge starts playing the dominant role on the loss enhancement. Between 4.35-4.65 μm, the loss of a TZBX10 glass fiber is between 50-100 dB/m. Therefore, this region should be a longwave limit for generating 10-dB bandwidth supercontinuum from a TZBX10 nonlinear fiber with a length between 10-20 cm.

5 Experimental results on mid-infrared generation in tellurite glass fibers

5.1 Early work on small-core tellurite glass fiber for mid-infrared nonlinear optics

With the rapid development of silica photonic crystal fibers (PCF), also called microstructured optical fibers, broadband $\chi^{(3)}$-based Kerr nonlinear optical processes, such as supercontinuum generation [47, 48] and optical parametric generation [49], have been experimentally realized using highly nonlinear, dispersion tailored silica PCFs. In order to extend these nonlinear optical processes into wavelength ranges that silica fiber cannot cover effectively, that is, the ultraviolet (UV, <400 nm) and mid-infrared regimes (>2 μm), non-silica glass highly nonlinear, dispersion tailored PCFs have been considered [50, 51].

Although a tellurite PCF with a mode area of 21.2 μm^2 has been reported as the world's first tellurite PCF in 2003 [51], the first work on using tellurite PCFs for mid-infrared nonlinear optics appeared in 2006 [52], using a single-mode, highly nonlinear tellurite PCF with an effective mode area of 2.6 μm^2 [53]. Fig.10 (a) shows scanning electron microscope (SEM) images of the cross-section of this small-core tellurite PCF. A triangular core with a diameter of ~2.6 μm is isolated from the outer jacket by three 7.4±0.2 μm long and 180±20 nm thin struts. Since the three thin supporting struts have a width that is much smaller and a length that is much larger than the wavelength of light, the core can be considered essentially as an air-suspended high-index glass rod.

The calculated group velocity dispersion curve of such an air-suspended-core (ASC) fiber and the material dispersion of the base glass ($75TeO_2$-$20ZnO$-$5Na_2O$, mol.%) are illustrated in Fig.10 (b). Due to the strong waveguide dispersion introduced by the small core and the high index contrast between the glass and the air surrounding the glass core, the zero dispersion wavelength (ZDW) of the ASC fiber is located at 1.46 μm, and thus is shifted considerably towards shorter wavelengths compared to the ZDW of 2.15 μm in the bulk glass.

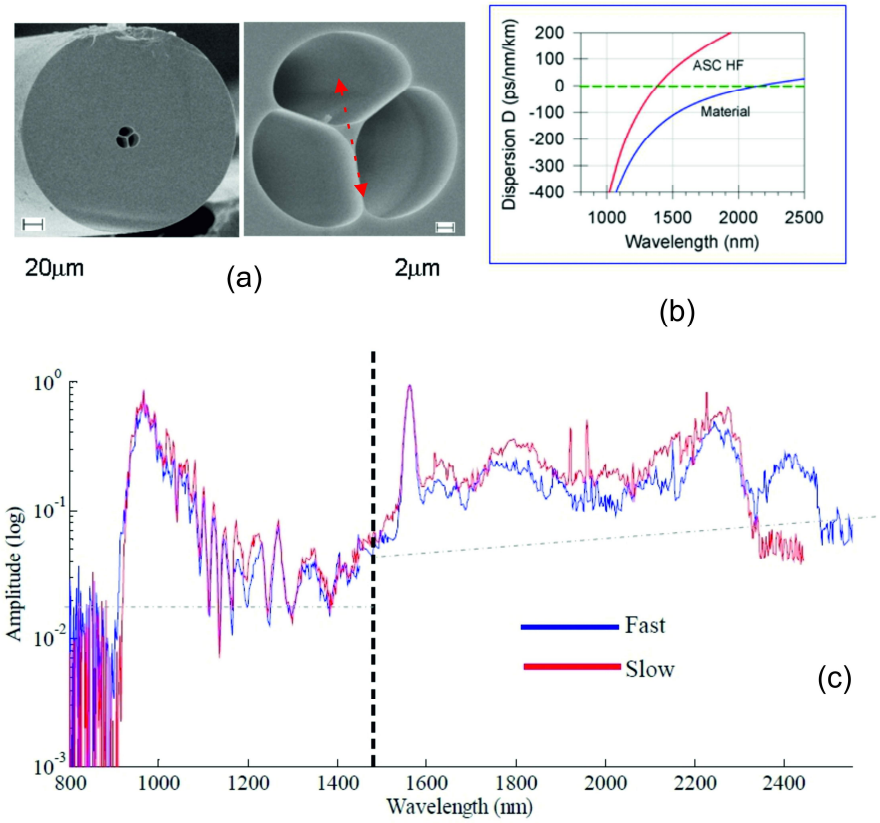

Fig. 10. (a) SEM photos of fiber cross-sectional structure of the ASC fiber. The arrow shows the direction of the fast axis of the fiber. (b) Dispersion curves of the ASC fiber and the bulk material. (c) Output supercontinuum spectra with 30 mW output power generated from a 22 cm length of this fiber, pumped at 1.56 μm wavelength on the fast and slow polarization axes, respectively. The vertical dashed line at 1.46 μm indicates the ZDW of the fiber.

Experimental observations as well as corresponding numerical simulations indicated that the fiber was effectively single-moded beyond 1 μm wavelength [53]. A small effective mode area A_{eff} of 2.6 μm^2 was calculated from the simulation result. Using the Boskovic method [54, 55], the fiber nonlinearity $\gamma = 2\pi n_2/(\lambda \cdot A_{eff})$, where n_2 is the nonlinear refractive index of the fiber core material, λ the operation wavelength and A_{eff} the effective mode area of the fiber core, respectively, was measured to be 280 ± 30 $W^{-1}km^{-1}$ at 1.55 μm, which is ~280 times higher than that of standard single mode silica optical fiber (Corning SMF28). Using the cutback method, the fiber attenuation was measured to be 2.0 dB/m at 1.55 μm.

Using a 1.56 μm femtosecond laser generated from a tunable optical parametric oscillator (OPO) as the pump source, broadband supercontinuum was observed from the tellurite ASC fiber [52]. The pulse duration of the OPO output was

measured to be 200 fs. The average output power from the OPO was ~160 mW, corresponding to a peak power of ~11.7 kW at 1.56 μm or equivalently to 2.1 nJ energy per pulse, with a spectral width (full width at half maximum (FWHM)) of ~15 nm. The pump wavelength was thus chosen in the anomalous dispersion region of the fiber but close to the ZDW, which is the standard arrangement for broadband supercontinuum generation [56]. As the laser pulses propagate along the fiber, they undergo sudden spectral broadening by soliton fission, followed by further generation of long-wavelength components via Raman-induced soliton self-frequency shifting. At the same time these solitons also create phase-matched dispersive waves at short wavelengths below the ZDW. Fig.10 (c) illustrates the observed broadband supercontinuum with an output power of 30 mW generated in this experiment with a tellurite ASC fiber of 22 cm length. Slightly different spectra were obtained when launching the pump light with different polarizations into fiber, in particular with polarizations parallel and perpendicular to the fast axis of the fiber (as shown in Fig. 10 (a)), suggesting a weak birefringence arising from the triangular fiber core. All in all, broadband supercontinuum from 0.9-2.5 μm was observed and it was the first report of generating mid-IR supercontinuum from a non-silica glass fiber.

In 2008, Domachuk et al. [40] used a similar ASC tellurite fiber and obtained a record 4000 nm bandwidth supercontinuum. This fiber was made of $75TeO_2$-$12ZnO$-$5PbO$-$3PbF_2$-$5Nb_2O_5$ and had a hexagonal air-suspended core with a diameter of 2.5 μm and a ZDW of 1380 nm. An OPO generating pulses at 1550 nm wavelength with 110 fs width at a repetition rate of 80 MHz was used to launch 150 mW of power at the fiber input. The supercontinuum measured at -45 dBm extended from 789 nm to 4870 nm, demonstrating the significant potential of tellurite glass fibers for applications all across the atmospheric transmission window up to 5 μm wavelength. However, because of the large water-induced absorption in the tellurite material of this fiber, a very short length of 8 mm of fiber was employed in the experiment, making the experimental alignment difficult while still leading to a significant slope towards lower power spectral density at the long wavelength edge.

5.2 Dehydrated small-core tellurite glass fiber

In order to improve on these early results on mid-infrared supercontinuum generation in tellurite fibers, two modifications to the fiber should be considered. (i) Using dehydrated glass, as described in Section 4 of this chapter, will significantly reduce absorption beyond 3 μm wavelength and will thus allow for the use of longer lengths of fiber and the generation of supercontinuum spectra with flatter power spectral densities. (ii) The near-symmetric cores of the fibers employed in the experiments described above limit the range of dispersion profiles that can be achieved. In particular, while the ZDW can be shifted continuously towards shorter wavelengths, it is generally not possible to also achieve a flat dispersion curve

over a broad wavelength range, that is, a low dispersion slope, which would further benefit efficient supercontinuum generation.

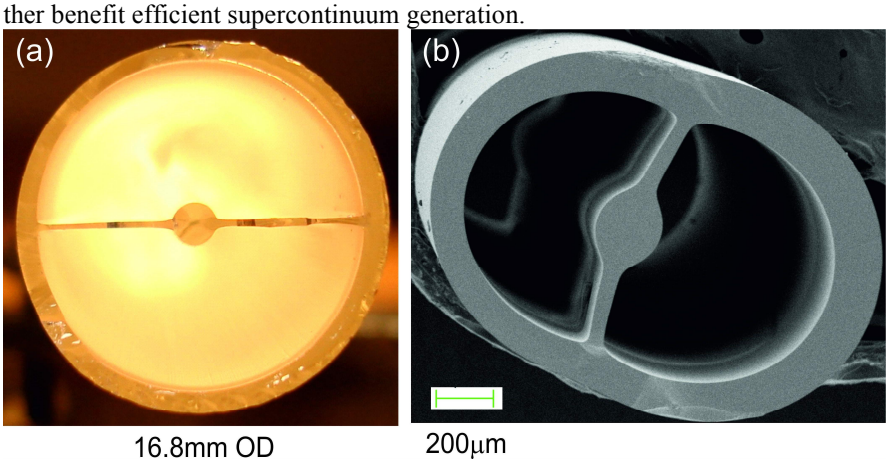

Fig. 11. (a) Photograph of extruded dehydrated TZBX1 preform and (b) SEM image of elongated cane for fiber drawing

To address these issues, a dehydrated TZBX1 glass-based PCF ($70TeO_2$-$20ZnO$-$9BaO$-$BaCl_2$ mol.%) with an elliptical air-suspended-core was fabricated [57]. A preform with one air-suspended core (see Fig.11 (a)) was made by extruding a dehydrated TZBX1 billet. A cane with a long axis diameter of 1.62 mm (see Fig.11 (b)) was then elongated from this structured preform. Next, the cane was inserted into an extruded jacket tube and this ensemble was then drawn into an ASC fiber with an elliptical core (see Fig.12 (a) & (b)). The elliptical core has a height (h) of 1.8 μm and a width (w) of 7.8 μm. The core exhibits strong birefringence, as shown by the calculated dispersion curves of the fundamental TE and TM polarized modes in Fig. 12 (c). The ZDW of the fundamental TE mode is located at 1.48 μm. Comparing the dispersion profile of this mode with that of Fig. 10 (b) for a symmetric-core ASC fiber, one notices that lower dispersion values are achieved over a broad bandwidth with this elliptical core fiber.

Supercontinuum generation with 90 fs, 1500 nm wavelength pump pulses of up to 1.12 nJ energy, similar to above, was investigated experimentally [57]. With 15 cm of fiber spectral broadening to ~3 μm was observed, but further broadening was limited by the available pump power.

With the same fiber, nonlinear broadening with a mid-infrared pump at 2.4 μm was also demonstrated. A linearly polarized OPO with a pulse duration of ~90 fs, a repetition rate of 80 MHz and a maximum average power of 290 mW at 2.4 μm was used as the pump source. The pump pulses were launched into a 3 cm long TZBX1 ASC fiber. For this fiber, the pump is therefore located deep inside the anomalous dispersion region, resulting in the generation of low order solitons by the pump pulses, which are then moving to longer wavelengths by Raman-induced self-frequency shifting, as can be seen clearly in Fig.13. The maximum launched average power was 48.6 mW, which corresponds to a peak power of 6.8 kW and a

pulse energy of 0.61 nJ. Even at these low, sub-nJ pulse energies, spectral broadening beyond 3.0 μm is readily observed with this dehydrated tellurite fiber.

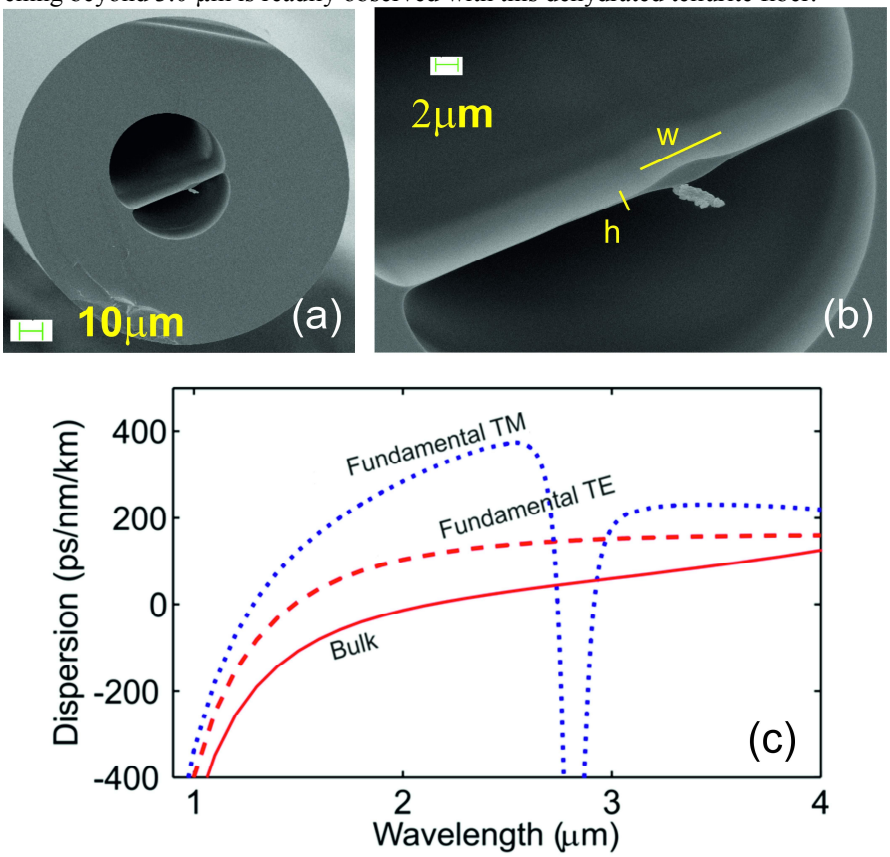

Fig. 12. (a) & (b) SEM images of the cross-section of fabricated TZBX1 elliptical ASC fiber. (c) Corresponding calculated dispersion profiles.

Further broadening of the mid-IR supercontinuum can be expected in fibers fabricated from the latest low-loss dehydrated TZBX10 glass, which will reduce losses in the 3-4 μm wavelength region by another factor of 10, see Section 4 above. Moreover, the dispersion profile can be further optimized using the design degrees of freedom offered by the elliptical core ASC geometry [57]. Work in this area is still ongoing at the time of writing.

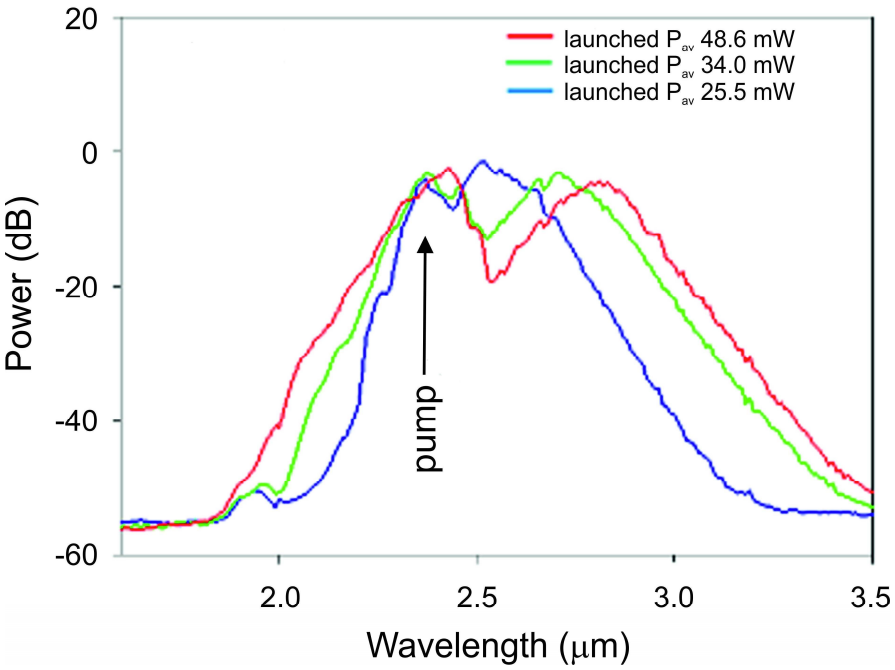

Fig. 13. Measured mid-infrared soliton dynamics in a 3 cm length of the ASC fiber of Fig. 12 pumped at 2.4 μm.

5.3 Power limitations in small-core tellurite glass fibers

Power scaling is a highly desirable performance characteristic of a fiber laser, and for many applications the achievable output power of the generated supercontinuum is more important than, for example, the spectral bandwidth. However, in all the small-core dispersion-tailored tellurite glass fiber experiments discussed above, the demonstrated mid-IR supercontinuum output power remained below 100 mW. This was partially limited by the attenuation located at 3-4 μm due to the water impurity of the material, but more importantly by the small size of the fiber core which leads to a low damage threshold for the fiber facet and thus limits the maximum pulse peak power and energy that can be launched into the fiber without destroying it.

For the tellurite ASC fiber discussed above in Section 5.1, the damage threshold was established using a 1.06 μm Yb-doped all-fiber master oscillator power amplifier (MOPA) with pulse duration of 20 ps and repetition rate of 14.4 MHz. Damage of the ASC fiber facet was observed under a launched average power of 140 mW, corresponding to a peak power of 390 W [58]. Fig. 14 shows optical mi-

croscope images of the tellurite ASC fiber before and after the facet was damaged. It is seen that the fiber core disappeared after the launched power exceeded the threshold, while the three supporting glass spokes still survived. The damage intensity is estimated to be 18.7 GW/cm^2. This is consistent with the reported surface damage threshold of tellurite bulk glasses, 15–20 GW/cm^2 using a Nd:YAG laser at 1.064 μm with a similar pulse duration of 25 ps [59]. As a comparison, under similar conditions the surface damage threshold of bulk silica glass is above 300 GW/cm^2 [60]. In order to significantly increase the achievable mid-IR supercontinuum power, tellurite fibers with much larger core sizes must therefore be employed.

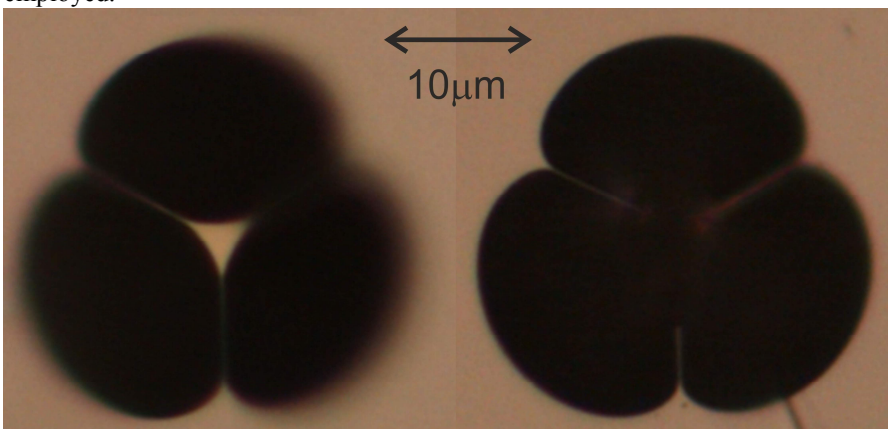

Fig. 14. Optical microscope images of the input facet of the tellurite ASC fiber before (left) and after (right) the damage caused by exceeding the laser power damage threshold.

5.4 Supercontinuum generation in large-mode-area tellurite glass fiber

Power scaling of common fiber lasers, such as rare-earth-doped fiber lasers or Raman fiber lasers, is routinely realized by using single-mode large-mode-area (LMA) fibers. The same concept also provides a feasible solution for achieving power scaling of broadband supercontinuum laser sources. Because the laser damage thresholds of non-silica glasses, such as tellurite glasses, fluoride glasses and chalcogenide glasses, are much lower than that of silica, it is especially important to develop non-silica glass LMA fibers for achieving medium- or high-level output power [61].

Figure 5(b) already showed a tellurite preform with three rings of holes surrounding a solid core that was made by extrusion. The preform has an outer diameter (OD) of 15.9 mm, a hole diameter of 1.0 mm, and hole-separation of 2.2 mm. The preform was directly drawn into fiber with 410±10 μm OD. Fig.15 (a) shows

an SEM image of the cross-section of this tellurite fiber with ~80 μm core diameter. The fiber has a uniform hole spacing Λ of 53 μm. Due to effects such as temperature gradients in the radial direction, surface tension and residual air-pressure inside the holes during the fiber-drawing process, the average hole diameter d_i (where i is the ring number counted from the core outwards, i=1 to 3) was reduced from d_1=28.1 μm for the inner ring to d_2=23.3 μm for the middle ring and d_3=13.8 μm for the outer ring of holes, corresponding to d_i/Λ ratios of 0.53, 0.44 and 0.26 respectively. Note that for all three rings the d_i/Λ ratios deviated from the initial value of 0.454 within the preform.

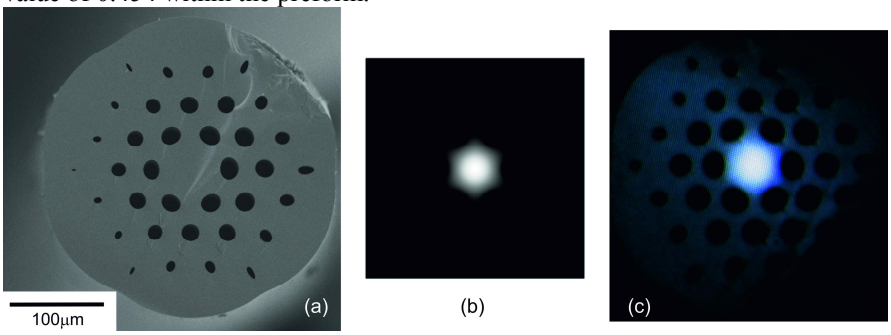

Fig. 15. (a) SEM image of the cross-section of the tellurite LMA PCF; (b) simulated mode profile of the fundamental mode (LP_{01}) at 1.55 μm; (c) the observed near-field mode profile at 1.55 μm from the fabricated tellurite LMA PCF. All three plots are on the same scale.

It is well known from theoretical investigations that a PCF supports only the fundamental fiber mode at all wavelengths if it has an infinite cladding containing an infinite number of rings of triangularly arranged holes with a ratio of hole diameter to hole spacing, d/Λ, of less than 0.40-0.45. This is often referred to as endlessly single-mode behavior [62], one of the unique optical properties of PCFs. For a practical PCF with a finite holey cladding and a finite number of air-filled holes, higher-order modes are more likely to be observed, especially in short fiber lengths [63]. Increasing the discrimination between the confinement losses (CLs) of the fundamental mode LP_{01} and the first higher order mode LP_{11} becomes the practical criterion for realizing single-mode operation in a PCF.

That the above tellurite LMA PCF was effectively single-moded was first confirmed by numerical simulations. The simulations predicted that the fundamental mode (LP_{01}) (as shown in Fig.15 (b)) and the first higher-order mode (LP_{11}) have a CL of ~10^{-4} dB/m and ≥3 dB/m at 1.55 μm, respectively. The ratio of the confinement losses of the fundamental mode to the first higher order mode at 1.55 μm is ~10^{-5}, indicating that only the fundamental mode LP_{01} can be observed at 1.55 μm if the fiber is sufficiently long. Further numerical simulations of this LMA PCF show that the ratio of the CL of the LP_{01} mode to that of the LP_{11} mode is ~10^{-4} in the whole range of 1-3 μm, while the CL of the LP_{11} mode is more than 1dB/m. This indicates that this LMA PCF has a broad bandwidth of more than

one octave for single-mode operation, while conventional single-mode optical fibers only operate over one octave of bandwidth [61], namely at normalized frequencies V ranging between 1.2 and 2.4 where $V = 2\pi a\sqrt{n_{core}^2 - n_{clad}^2} / \lambda$, where a is the fiber core radius, λ the wavelength of light, and n_{core} and n_{clad} the core and cladding refractive index, respectively.

Robust guidance with a hexagonally symmetric mode profile was observed at 1.55 μm (see Fig.15(c)) in a 1.50 m long tellurite PCF. During this measurement the fiber was kept effectively straight, i.e., with an estimated bending radius of ~2 m, to minimize the influence of bending loss on the fundamental mode. The observed mode profile was in good agreement with the simulated fundamental (LP_{01}) mode (see Fig.15 (b)). The beam quality factor M^2 was measured as 1.3±0.1 at 1.55 μm. Both experimental and simulation results indicated the effective single-mode operation of the fiber [61].

From the simulations an effective mode area A_{eff} of 3000±200 μm^2 was calculated for the fundamental mode [61]. This is the largest mode area reported so far in a single mode non-silica glass fiber, and is comparable to the effective mode area in silica glass LMA PCFs, for example, the 3160 μm^2 reported in Ref. [64]. The propagation attenuation of this tellurite LMA PCF was measured as 2.9±0.1 dB/m at 1.55 μm using the cutback method. The effective fiber nonlinearity γ of the LMA PCF was calculated to be 0.23 $W^{-1}km^{-1}$ at 1.55 μm. Because of the large core size the dispersion profile is effectively the same as its material dispersion, as illustrated in Fig.10 (b), with a zero-dispersion-wavelength and a relatively flat dispersion slope at 2.15 μm.

Experimental work on generating broadband mid-IR supercontinuum from the tellurite LMA PCF was carried out using a tunable femtosecond pulsed optical parametric amplifier (OPA) with a repetition rate of 1 kHz and a pulse duration of ~120 fs [61]. The idler beam from the OPA at 2.15 μm was launched into a straight piece of the fiber of 9 cm length using a microscope objective with an NA of 0.1. This pump wavelength was chosen because it coincides with the fiber ZDW. Supercontinuum generation was then investigated at average pump powers of 2.4 mW to 15.2 mW, measured before the launch into the fiber. The measured output spectra showed significant broadening towards shorter wavelengths down to about 1 μm. Unfortunately this experiment did not record the spectrum above 2.5 μm because of the long-wavelength limit of the used detector, a cooled extended InGaAs photodiode, and thus the full extent of the supercontinuum into the mid-IR region is unknown. However, the supercontinuum output power was measured at the end of the LMA fiber of 6.0±0.2 mW for an incident pump power of 15.2 mW, showing high conversion efficiency from the pump to the supercontinuum [61].

Most importantly, while the average power used in this experiment was relatively modest, the low laser repetition rate compared to the experiments discussed above in the small-core fibers (1 kHz here compared to 80 MHz) means that the individual pulses launched into the LMA fiber had peak powers and pulse energies several orders of magnitude higher than what could be used in the small-core ASC

fibers because of their low damage threshold. In particular, at the maximum incident pump average power of 15.2 mW, the pulse energy reached 15.2 μJ and the peak power was 127 MW. No facet damage of the tellurite LMA fiber was observed during these experiments, demonstrating the potential for power scaling of mid-IR supercontinuum generation in tellurite fibers by moving towards large-core low-NA fiber structures.

6 Outlook

Table 3. Summary of using tellurite PCFs for generating mid-IR supercontinuum. The long wavelength cutoff in the experiments marked with + was not properly resolved because of detector limitations.

fiber	Effective mode area (μm^2)	water-induced attenuation at water peak (at 3.3 μm)	Fiber length (cm)	Launched Pulse energy (J)	Launched Peak power (W)	Spectral span (μm) (20 dB width)	Ref.
ASC PCF with triangular core	2.6	~1400	22	$2.1x10^{-9}$	$11.7x10^{3}$	$0.9\text{-}2.5^{+}$	[52]
ASC PCF with hexagonal core	1.7	~1400	0.8	$1x10^{-9}$	$8.5x10^{3}$	0.79-4.87	[40]
ASC PCF with elliptical core	3.9	~70	3	$0.61x10^{-9}$	$6.8x10^{3}$	2.2-3.1	[57]
LMA PCF	3000	~1400	9	$15.2x10^{-6}$	$127x10^{6}$	$1.0\text{-}2.5^{+}$	[61]

Table 3 summarizes the results that we have discussed in this chapter on using tellurite glass nonlinear PCFs for generating mid-IR supercontinuum. Supercontinuum generation in a small-core tellurite fiber was first demonstrated in 2006 [52]. Spectral broadening up to nearly 5 μm has been observed in a similar fiber structure [40], but only impractically short fiber lengths could be used because of water absorption. A small-core fiber made from dehydrated tellurite glass has also been demonstrated [57] with a novel elliptical core geometry allowing for better dispersion control. In all these small-core fibers the maximum pulse energy and peak power were limited by the fiber damage threshold to about 1 nJ and 10 kW, respectively. A large mode area tellurite fiber [61] was demonstrated that could support 3-4 orders of magnitude higher powers.

Based on these results, it is expected that using 0.1-1 m lengths of dehydrated LMA tellurite fibers with a water-induced loss of less than 10 dB/m at 3.3 μm will allow for the generation of flat 2-5 μm supercontinuum spectra with peak output powers of 100 MW.

Acknowledgments

The authors thank Prof. P. Petropoulos, Prof. D. J. Richardson, Mr. K. E. Frampton, Mr. N. M. White, Dr. M. Segura, Dr. J. Shi, and Dr. W. Loh of the Optoelectronics Research Centre, University of Southampton, for their contributions.

Xian Feng also thanks Prof. S. Tanabe and Dr. J. S. Wang for fruitful discussions in the early stages of developing tellurite glass fibers.

References

[1] Schliesser A, Picqué N, Hänsch T W (2012) Mid-infrared frequency combs. Nature Photonics **6**: 440–449

[2] Sorokin E, Sorokina I T, Mirov M S, Fedorov V V, Moskalev I S, Mirov S B (2010) Ultrabroad continuous-wave tuning of ceramic Cr:ZnSe and Cr:ZnS lasers. Paper presented at the Adv. Solid-State Photon., San Diego, CA, USA

[3] IPG Photonics, TM:ZnSe/S SERIES, http://www.ipgphotonics.com/Collateral/Documents/English-US/TM_ZnSE_S_Series_IPG_datasheet.pdf. Accessed 29 Jun 2015

[4] Razeghi M, Bandyopadhyay N, Bai Y, Lu Q, Slivken S (2013) Recent advances in mid infrared (3-5μm) Quantum Cascade Lasers. Opt Mater Express 3: 1872-1884

[5] Bandyopadhyay N, Bai Y, Tsao S, Nida S, Slivken S, Razeghi M (2012) Room temperature continuous wave operation of $\lambda \sim$ 3-3.2 μm quantum cascade lasers. Appl Phys Lett **101**: 241110

[6] Zhu X, Peyghambarian N (2010) High-Power ZBLAN Glass Fiber Lasers: Review and Prospect, Advances in OptoElectronics **2010**: Article ID 501956

[7] Jackson S D (2012) Towards high-power mid-infrared emission from a fibre laser, Nature Photonics **6**: 423–431

[8] Ebrahimzadeh M (2003) Mid-Infrared Ultrafast and Continuous-Wave Optical Parametric Oscillators, Solid-State Mid-Infrared Laser Sources. In: Sorokina I T, Vodopyanov, K L (ed) Topics in Applied Physics, Volume 89, Solid-State Mid-Infrared Laser Sources, Springer-Verlag, Berlin Heidelberg, p 184-224

[9] Russell P St J (2003) Photonic crystal fibers. Science **299**: 358–362

[10] Ranka J K, Windeler R S, Stentz A J (2000) Visible continuum generation in air-silica microstructure optical fibers with anomalous dispersion at 800 nm. Opt Lett **25**: 25–27

[11] Serkland D K, Kumar P (1999) Tunable fiber-optic parametric oscillator. Opt Lett **24**: 92-94

[12] Cundiff S T, Ye J (2003) Colloquium: Femtosecond optical frequency combs. Rev Mod Phys **75**: 325-342

[13] Szigeti B (1949) Polarisability and dielectric constant of ionic crystals. Trans. Faraday Soc **45**: 155-166

[14] Boniort J Y, Brehm C, DuPont PH, Guignot D, Sergent C Le (1980) Infrared glass optical fibers for 4 and 10 micron bands. Paper presented at 6th European Conference on Optical Communication, University of York, UK, 16-19 Sept 1980

[15] Poulain M, Poulain M, Lucas J, Brun P (1975) Verres fluores au tetrafluorure de zirconium proprietes optiques d'un verre dope au Nd^{3+}. Mat Res Bull **10**: 243–246

[16] Kapany N S, Simms R J (1965) Recent developments of infrared fiber optics. Infrared Phys **5**: 69–75

[17] Mori A, Masuda H, Shikano K, Shimizu M (2003) Ultra-Wide-Band Tellurite-Based Fiber Raman Amplifier. IEEE J Lightwave Technol **21**: 1330-1306
[18] Mizunami, Iwashita H, Takagi K (1993) Gain saturation characteristics of Raman amplification in silica and fluoride glass optical fibers. Opt Comm **97**: 74–78
[19] Szebesta D, Davey S T, Williams J R, Moore M W (1993) OH absorption in the low loss window of ZBLAN(P) glass fibre. J. Non-Crystalline Solids **161**: 18–22
[20] Sanghera J S, Brandon Shaw L, Aggarwal I D (2009) Chalcogenide Glass-Fiber-Based Mid-IR Sources and Applications. IEEE J Sel Top Quantum Electron **15**: 114-119
[21] Slusher R E, Hodelin J, Sanghera J S, Shaw L B, Aggarwal I D (2004) Large Raman gain and nonlinear phase shifts in high-purity As2Se3 chalcogenide fibers. J Opt Soc Am B **21**: 1146–1155
[22] Vasilev A V, Devyatykh G G, Dianov E M, Guryanov A N, Laptev A Yu, Laptev A Yu, Plotnichenko V G (1993) Two-layer chalcogenide-glass optical fibers with optical losses below 30 dB/km. Quantum Electron **23**: 89-90
[23] Wang J S, Vogel E M, Snitzer E (1994) Tellurite glass: a new candidate for fiber devices. Opt Mater **3**: 187-203
[24] Ghosh G (1995) Sellmeier coefficients and chromatic dispersions for some tellurite glasses. J Am Ceram Soc **78**: 2828-30
[25] Mitachi S, Miyashita T, Kanamori T (1981) Fluoride-glass-cladded optical fibres for mid-infra-red ray transmission. Electron Lett **17**: 591-592
[26] Kanamori T, Sakaguchi S (1986) Preparation of elevated NA fluoride optical fibers. Japan J Appl Phys **25**: L468-L470
[27] Sakaguchi S, Takahashi S (1987) Low-loss fluoride optical fibers for midinfrared optical communication. J Lightwave Technol **5**: 1219-28
[28] Tran D C, Fisher C F, Sigel G H (1982) Fluoride glass preforms prepared by a rotational casting process. Electron Lett **18**: 657-8
[29] Lu G, Aggarwal I (1987) Recent advances in fluoride glass fiber optics in the USA. Mater Sci Forum **19-20**: 375-380
[30] Feng X, Mairaj A K, Hewak D W, Monro T M (2005) Nonsilica Glasses for Holey Fibers. J Lightwave Technol **23**: 2046-2054
[31] Roeder E (1971) Extrusion of glass. J Non-Crystall Solids **5**: 377-388
[32] Stanworth J E (1952) Tellurite Glasses. Nature **169**: 581-582
[33] Rawson H (1967) Inorganic Glass Forming Systems. Academic Press, London, New York
[34] Yakhkind A K (1966) Tellurite Glasses. J Am Ceram Soc **49**: 670-675
[35] Dorofeev V V, Moiseev A N, Churbanov M F, Snopatin G E, Chilyasov A V, Kraev I A, Lobanov A S, Kotereva T V, Ketkova L A, Pushkin A A, Gerasimenko V V, Plotnichenko V G, Kosolapov A F, Dianov E M (2011) High-purity TeO_2–WO_3–(La_2O_3, Bi_2O_3) glasses for fiber-optics, Opt Materials **33**: 1911–1915
[36] Feng X, Flanagan J C, Frampton K E, Petropoulos P, White N M, Price J H V, Loh, W H, Rutt H N, Richardson D J (2008) Developing single-mode tellurite glass holey fiber for infrared nonlinear applications. Adv Sci Technol **55**: 108–117
[37] Humbach O, Fabian H, Grzesik U, Haken U, Heitmann W (1996) Analysis of OH absorption bands in synthetic silica. J Non-Crystall Solids **203**: 19–26
[38] France P W, Carter S F, Williams J R, Beales K J, Parker J M (1984) OH-absorption in fluoride glass infra-red fibres. Electron Lett **20**: 607–608
[39] Feng X, Tanabe S, Hanada T (2001) Hydroxyl groups in erbium-doped germanotellurite glasses. J Non-Crystall Solids **281**: 48–54
[40] Domachuk P, Wolchover N A, Cronin-Golomb M, Wang A, George A K, Cordeiro C M B, Knight J C, Omenetto F G (2008) Over 4000 nm bandwidth of mid-IR supercontinuum generation in sub-centimeter segments of highly nonlinear tellurite PCFs. Opt Express **16**: 7161-7168
[41] Comyns A E (1989) Fluoride glasses. Wiley, Hoboken, NJ, USA

[42] Nagel S, MacChesney J B, Walker K (1982) An overview of the modified chemical vapor deposition (MCVD) process and performance. IEEE Trans Microwave Theory Tech **18**: 459–476
[43] O'Donnell M D, Miller C A, Furniss D, Tikhomirov V K, Seddon A B (2003) Fluorotellurite glasses with improved mid-infrared transmission. J. Non-Crystall Solids **331**: 48–57.
[44] Feng X, Shi J, Segura M, White N M, Kannan P, Loh W H, Calvez L, Zhang X, Brilland L (2013) Halo-tellurite glass fiber with low OH content for 2-5μm mid-infrared nonlinear applications. Opt. Express, **21**: 18949-18954
[45] Feng X, Shi J, Segura M, White N M, Kannan P, Calvez L, Zhang X, Brilland L, Loh W H (2013) Towards Water-Free Tellurite Glass Fiber for 2–5 μm Nonlinear Applications. Fibers **1**: 70-81
[46] Ebendorff-Heidepriem H, Kuan K, Oermann M R, Knight K, Monro T M (2012) Extruded tellurite glass and fibers with low OH content for mid-infrared applications. Opt Materials Express **2**: 432-442
[47] Ranka J K, Windeler R S, Stentz A J (2000) Visible continuum generation in air–silica microstructure optical fibers with anomalous dispersion at 800 nm. Opt Lett **25**: 25-27
[48] Dudley J M, Provino L, Grossard N, Maillotte H, Windeler R S, Eggleton B J, Coen S (2002) Supercontinuum generation in air–silica microstructured fibers with nanosecond and femtosecond pulse pumping. J Opt Soc Am B **19**: 765-771
[49] Chen A Y H, Wong G K L, Murdoch S G, Leonhardt R, Harvey J D, Knight J C, Wadsworth W J, Russell P St J (2005) Widely tunable optical parametric generation in a photonic crystal fiber. Opt Lett **30**: 762-764
[50] Monro T M, West Y D, Hewak D W, Broderick N G R, Richardson D J (2000) Chalcogenide holey fibres. Electron Lett **36**: 1998 – 2000
[51] Kumar V V R K, George A K, Knight J C, Russell P St J (2003) Tellurite photonic crystal fiber. Opt Express **11**: 2641-2645
[52] Delmonte T, Watson M A, O'Driscoll E J, Feng X, Monro T M, Finazzi V, Petropoulos P, Price J H V, Baggett J C, Loh W, Richardson D J, Hand D P (2006) Generation of mid-IR continuum using tellurite microstructured fiber. Paper presented at Conference of Lasers and Electro-Optics (CLEO) and Quantum Electronics and Laser Science Conference (QELS), Long Beach, California, USA 21-25 May 2006
[53] Feng X, Monro T M, Finazzi V, Moore R C, Frampton K, Petropoulos P, Richardson D J (2005) An extruded single-mode high-nonlinearity tellurite glass holey fibre. Electron Lett **41**: 835-837
[54] Boskovic A, Chernikov S V, Taylor J R, Gruner-Nielsen L, Levring O A (1996) Direct continuous-wave measurement of n_2 in various types of telecommunication fiber at 1.55 μm. Opt Lett **21**: 1966-1968
[55] Broderick N G R, Monro T M, Bennett P J, Richardson D J (1999) Nonlinearity in holey optical fibers: measurement and future opportunities. Opt Lett **24**: 1395–1397
[56] Dudley J M, Genty G, Coen S (2006) Supercontinuum generation in photonic crystal fiber. Rev Mod Phys **78**: 1135–1184
[57] Belal M, Xu L, Horak P, Shen L, Feng X, Ettabib M, Richardson D J, Petropoulos P, Price J H V (2015) Mid-infrared supercontinuum generation in suspended core tellurite microstructured optical fibers. Opt Lett **40**: 2237-2240
[58] Shi J, Feng X, Horak P, Chen K, Teh P S, Alam S, Loh W H, Richardson D J, Ibsen M (2011) 1.06μm picosecond pulsed, normal dispersion pumping for generating efficient broadband infrared supercontinuum in meter-length single-mode tellurite holey fiber with high Raman gain coefficient. J. Lightwave Techno **29**: 3461-3469
[59] Stegeman R, Jankovic L, Kim H, Rivero C, Stegeman G, Richardson K, Delfyett P, Guo Y, Schulte A, Cardinal T (2003) Tellurite glasses with peak absolute Raman gain coefficients up to 30 times that of fused silica. Opt Lett **28**: 1126–1128
[60] Stuart B C, Feit M D, Rubenchik A M, Shore B W, Perry M D (1995) Laser-Induced Damage in Dielectrics with Nanosecond to Subpicosecond Pulses. Phys Rev Lett **74**: 2248-2251

[61] Feng X, Loh W H, Flanagan J C, Camerlingo A, Dasgupta S, Petropoulos P, Horak P, Frampton K E, White N M, Price J H V, Rutt H N, Richardson D J (2008) Single-mode tellurite glass holey fiber with extremely large mode area for infrared nonlinear applications. Opt Express **16**: 13651-13656
[62] Birks T A, Knight J C, Russell P St J (1997) Endlessly single-mode photonic crystal fiber. Opt Lett **22**: 961-963
[63] Grassi A. M., Casagrandea F., D'Alessandroa M., Marinonia S., (2007) Single-modeness of short large mode area fibers: an experimental study. Opt Commun **273**: 127-132
[64] Dong L, Peng X, Li J (2007) Leakage channel optical fibers with large effective area. J Opt Soc Am B **24**: 1689-1697